Supplementary material: Diffuse axonal injury has a characteristic multidimensional MRI signature in the human brain

Dan Benjamini[a,b,c,*], Diego Iacono[b,c,d,e,f,g], Michal E. Komlosh[a,b,c], Daniel P. Perl[b,e], David L. Brody[b,d,h], Peter J. Basser[a,b]

[a]*The Eunice Kennedy Shriver National Institute of Child Health and Human Development, National Institutes of Health, Bethesda, MD, USA*
[b]*Center for Neuroscience and Regenerative Medicine, Uniformed Services University of the Health Sciences, Bethesda, MD, USA*
[c]*The Henry M. Jackson Foundation for the Advancement of Military Medicine (HJF), Bethesda, MD, USA*
[d]*Department of Neurology, F. Edward Hébert School of Medicine, Uniformed Services University, Bethesda, MD, USA*
[e]*Department of Pathology, F. Edward Hébert School of Medicine, Uniformed Services University, Bethesda, MD, USA*
[f]*Department of Anatomy, Physiology, and Genetics, F. Edward Hébert School of Medicine, Uniformed Services University, Bethesda, MD, USA*
[g]*Motor Neuron Disorders Unit, National Institute of Neurological Disorders and Stroke, National Institutes of Health, Bethesda, MD, USA*
[h]*Laboratory of Functional and Molecular Imaging, National Institute of Neurological Disorders and Stroke, National Institutes of Health, Bethesda, MD, USA*

Supplementary Methods

MRI acquisition

The acquisition of multidimensional data was done using echo planar imaging (EPI) readout according to the MADCO framework encoding scheme (Benjamini and Basser, 2016, 2018), and by varying the following three experimental parameters: the inversion time, τ_1, the echo time, τ_2, and the diffusion weighting, b, providing T_1-, T_2-, and diffusion-weighting, respectively.

The minimal values of the two timing parameters, τ_1 and τ_2, depend on the sample physical dimensions because of the varying imaging matrix size that is intended to keep the spatial resolution constant at 300 μm isotropic. We kept the minimal τ_1 and τ_2 relatively constant across the samples at $\tau_1 = 12.0 \pm 1.5$ and $\tau_2 = 10.5 \pm 0.8$, by adjusting the number of EPI segments as necessary (<8).

The three 1D distributions of T_1, T_2, and MD, were estimated, respectively, with the following data acquisition protocols: A 1D T_1-weighted data set ($b = 0$, $\tau_2 = 10.5$ ms) with 20 logarithmically sampled τ_1 values ranging from 12 to 980 ms by using an IR-DWI-EPI sequence; a 1D T_2-weighted data set (b=0) with 20 logarithmically sampled τ_2 values ranging from 10.5 to 125 ms by using a DWI-EPI sequence. For diffusion encoding, we used the isotropic generalized diffusion tensor MRI (IGDTI) acquisition protocol to achieve an efficient orientationally averaged DW signal (Avram et al., 2018) with the following parameters: 16 linearly sampled b-values ranging from 2,540 to 14,700 s/mm^2 in 3 directions, 14 linearly sampled b-values ranging from 4,140 to 14,700 s/mm^2 in 4 directions, and 9 linearly sampled b-values ranging from 8,260 to 14,700 s/mm^2 in 6 directions, using the efficient gradient sampling schemes in Table 2 in (Avram et al., 2018). This type of diffusion encoding increases the contrast given by local anisotropy and is not intended to measure the isotropic diffusion in the system. Additional diffusion parameters were gradient duration of $\delta = 4$ ms and diffusion time of $\Delta = 15$ ms.

The three 2D distributions of MD-T_1, MD-T_2, and T_1-T_2, were estimated, respectively, with the following data acquisition protocols (in conjunction with the *a priori* obtained 1D distributions as constraints): A 2D diffusion-T_1-weighted data set with 16 sampled combinations of inversion times and b-values within the aforementioned 1D acquisition range; a 2D D-T_2-weighted data set with 16 sampled combinations of echo times and b-values within the aforementioned 1D acquisition range; and a 2D T_1-T_2-weighted data set with 16 sampled combinations of inversion and echo times within the aforementioned 1D acquisition range.

The data were averaged 4 times to maintain high signal-to-noise ratio (SNR), which was always maintained above 100 (defined as the ratio between the average unattenuated signal intensity within a tissue region of interest, and the standard deviation of the signal intensity within the background). The sample temperature was set at 16.8°C.

Multidimensional MRI processing

The 2D T_1-T_2, MD-T_1, and MD-T_2 distributions were evaluated on logarithmically sampled grids using a previously described algorithm (Benjamini and Basser, 2016). The range for T_1 was 1 10,000 ms, the range for T_2 was 1 500 ms, and the range for MD was 0.0001 5 μ m^2/ms.

*Corresponding author. Phone: +1-301-435-3868
Email address: dan.benjamini@nih.gov (Dan Benjamini)

Two factors guided us in the search for injury-associated spectral ROIs: (1) we know the injury is primarily a WM injury, and (2) we know the T_1-T_2-MD range of what is deemed as normal WM from previous multidimensional MRI studies (and current results) (Benjamini and Basser, 2017; Pas et al., 2020). Our driving hypothesis was therefore that microscopic WM injury would affect the normal WM spectral component, and that the axonal injury spectral information would be found in the vicinity of the normal WM component. Based on this notion, we have identified a T_1-T_2-MD range, T_1=[91.03, 339.32] ms, T_2=[6.70, 34.85] ms, and MD=[0.004, 0.146] μ m^2/ms, in which we observed the presence of injury-associated spectral information. Because of normal biological variability and also potential fixation variability effects (i.e., PMI), different cases presented slightly different multidimensional distributions. We therefore performed further per-case adjustment to locate the most relevant portion of the spectra within the pre-selected T_1-T_2-MD range.

Because of the sparsity of TAI lesions in the CC, the injury-indicative spectral information is undetectable when looking at the multidimensional distributions averaged over the entire CC. However, those averaged distributions can be used to identify the border between normal and abnormal tissue within the aforementioned T_1-T_2-MD range. We applied an adaptive threshold to find the edge of the spectral peak that resides within the pre-defined T_1-T_2-MD range. That spectral peak is mostly normal WM tissue, and anything outside of that peak, as defined by the detected edges, was considered related to the axonal injury, and was defined as the spectral ROI. A schematic illustration of the process can be found in Fig. S1.

Immunohistochemistry

Primary antibodies used were amyloid precursor protein (APP, mouse antihuman monoclonal antibody clone 22c11, dilution 1:10, epitope retrieval time 10 minutes, MAB348; EMD Millipore, Burlington, MA), anti-ionized calcium-binding adapter molecule 1 (Iba-1, rabbit polyclonal, dilution 1:100, epitope retrieval time 10 minutes, Wako 016-20001; FUJIFILM Wako Pure Chemical Corporation, Osaka, Japan), myelin basic protein (MBP, 1:100, epitope retrieval time 10 minutes, ab62631; Abcam, Cambridge, MA), and antiglial fibrillary acidic protein (GFAP, mouse antihuman monoclonal antibody GA5 with bond heat-induced epitope retrieval, epitope retrieval time 10minutes, PA0026; Leica Biosystems, Wetzlar, Germany).

Repeatability and reproducibility assessment of Multidimensional MRI

Repeatability and reproducibility of the T_1-T_2, MD-T_1, and MD-T_2 TAI SC images were evaluated by repeating the multidimensional MRI acquisitions for Cases 1 and 2. For each of these subjects, the duplicate data sets were processed using the same pipeline and then compared. The TAI SC images of each of these cases were estimated twice, using the two independently acquired data sets. The resulting images were then compared using Bland-Altman plots to quantify the degree of repeatability and reproducibility (Bland and Altman, 1986). Specifically, to avoid including insignificant voxels, we first eliminated all voxels that had very small intensity values (< 0.0001). If one considered the duplicate acquisitions of each of the cases as paired measurements, the Bland-Altman plot display the difference of the two paired measurements against the mean of the two measurements. The standard deviation of the measurement error in Case 1 was 5.3 for T_1-T_2 injury SC, 5.5 for MD-T_1 injury SC, and 5.3 for MD-T_2 injury SC (Fig. S2), and in Case 2 it was 4.8 for T_1-T_2 injury SC, 4.3 for MD-T_1 injury SC, and 6.5 for MD-T_2 injury SC (Fig. S3).

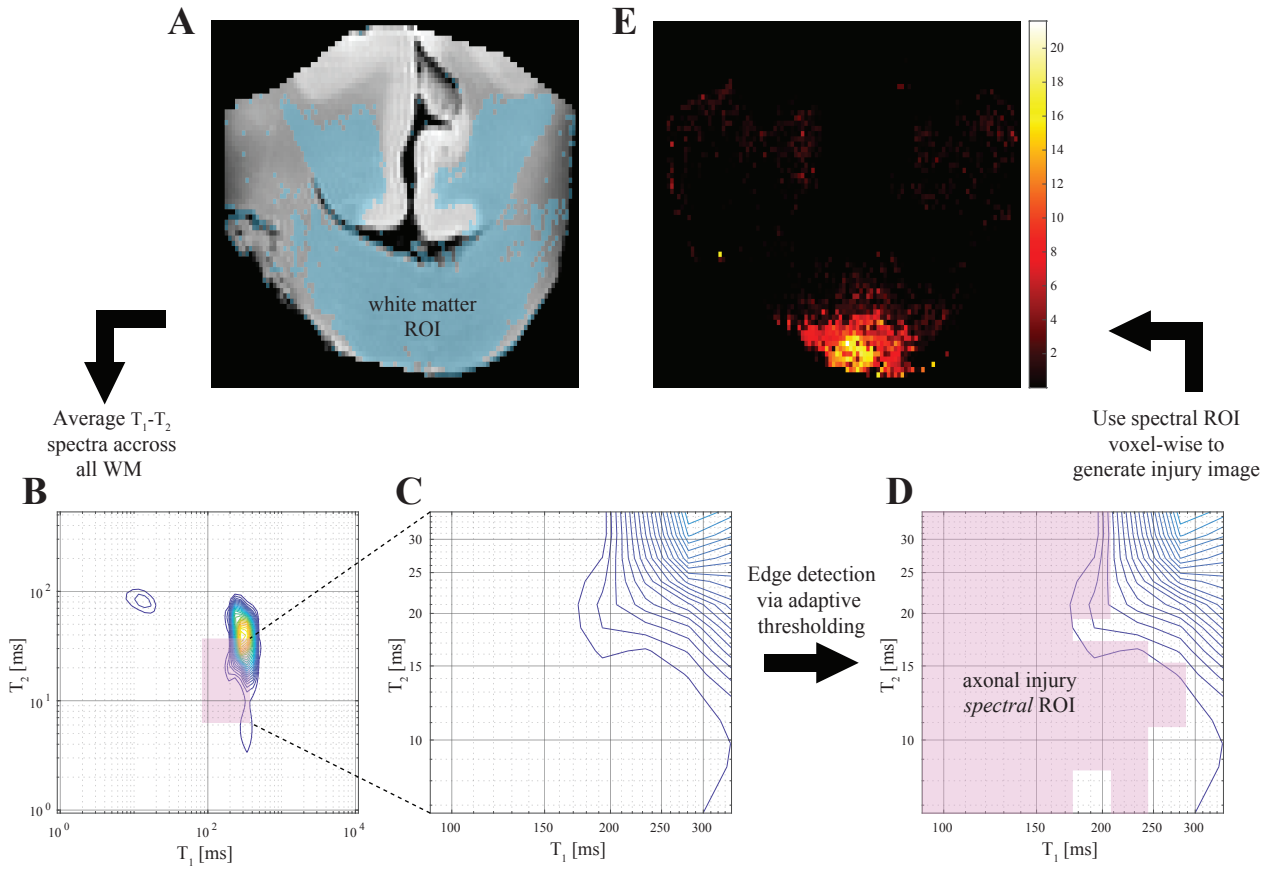

Figure S1: A schematic illustration of the spectral ROI definition process, shown on the T_1-T_2 data set of Case 4. (A) White matter segmented based on the FA, and all T_1-T_2 distributions are averaged across the WM ROI, yielding (B) an WM-average T_1-T_2 spectrum. (C) A magnification of the pre-selected T_1-T_2 range. (D) An edge detection procedure (using a standard adaptive threshold algorithm) in the spectral domain is performed to identify the edge of the normal-appearing WM spectral component. Once that edge is found, the spectral ROI is defined such that it would exclude the normal WM spectral information and include the rest of the T_1-T_2 range, based on our hypothesis that the injury-associated spectral information would be found in the vicinity of the normal WM component. (E) The spectral ROI is then applied voxel-wise on the T_1-T_2 distributions data set, which yields an image of the axonal injury spectral component.

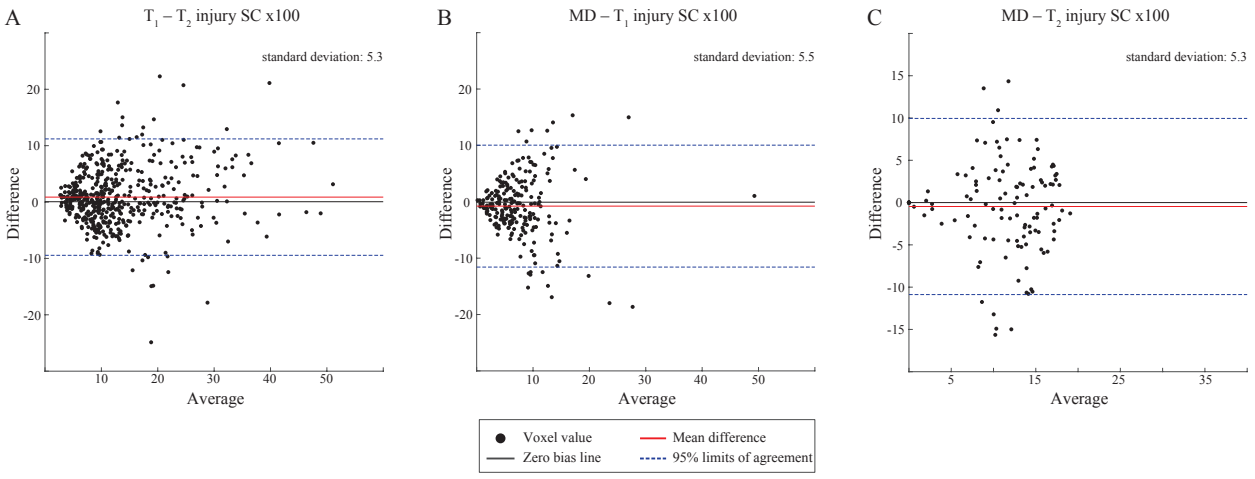

Figure S2: Repeatability of multidimensional MRI pipeline used in the study. Two separate multidimensional datasets were acquired from the same ex vivo tissue block (Case 1) using identical acquisition parameters. The (A) T_1-T_2, (B) MD-T_1, and (C) MD-T_2 TAI SCs were then calculated in each voxel for each dataset and compared using Bland-Altman plots. High agreement between the two repeated acquisitions was observed for T_1-T_2, MD-T_1, and MD-T_2.

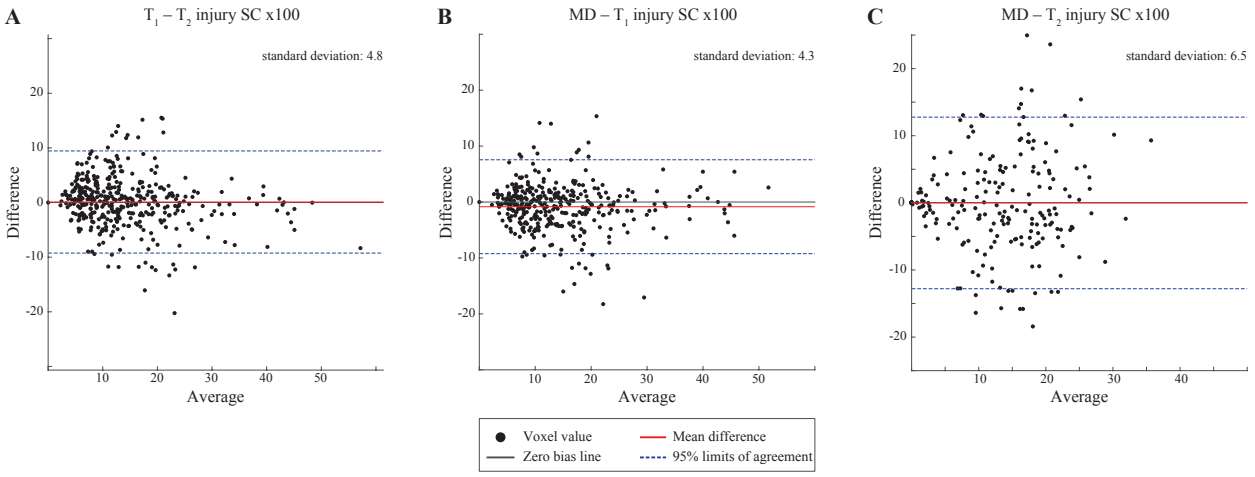

Figure S3: Repeatability of multidimensional MRI pipeline used in the study. Two separate multidimensional datasets were acquired from the same ex vivo tissue block (Case 2) using identical acquisition parameters. The (A) T_1-T_2, (B) MD-T_1, and (C) MD-T_2 TAI SCs were then calculated in each voxel for each dataset and compared using Bland-Altman plots. High agreement between the two repeated acquisitions was observed for T_1-T_2, MD-T_1, and MD-T_2.

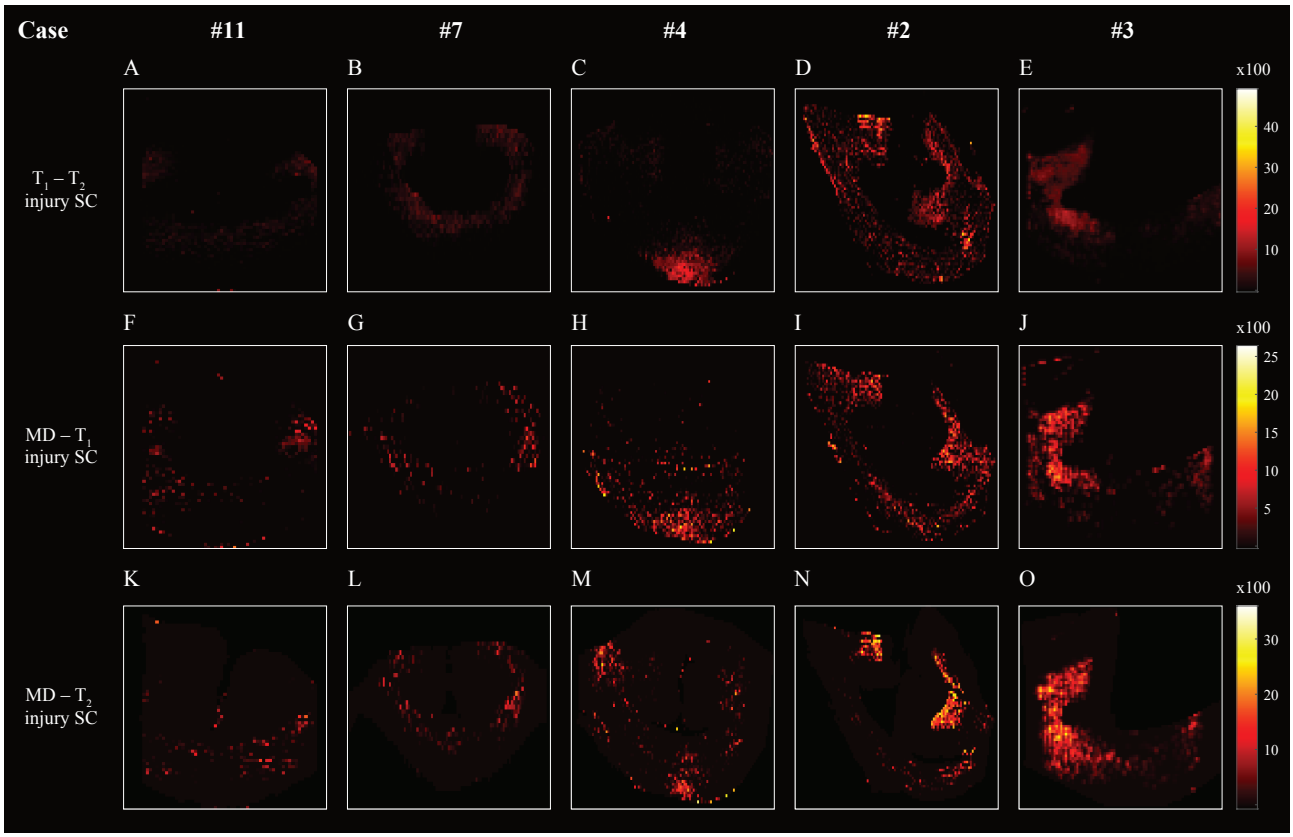

Figure S4: Multidimensional injury images of several examined cases with increased severity. (A) T_1-T_2, (F) MD-T_1, and (K) MD-T_2 injury images of control CC (Case 11) show negligible image intensities. (B) T_1-T_2, (G) MD-T_1, and (L) MD-T_2 TAI images of nonfatal TBI with mild APP staining CC (Case 7) show slightly increased image intensities, compared to Case 11. (C) T_1-T_2, (H) MD-T_1, and (M) MD-T_2 injury images of fatal TBI with severe APP staining CC (Case 4) show clear localization of extensive WM damage. (D) T_1-T_2, (I) MD-T_1, and (N) MD-T_2 injury images of fatal TBI with severe APP staining CC (Case 2) show damage mostly at the GM-WM interface. (E) T_1-T_2, (J) MD-T_1, and (O) MD-T_2 injury images of fatal TBI with severe APP staining CC (Case 3) show bilateral damage with strong presence in the left side of the CC.

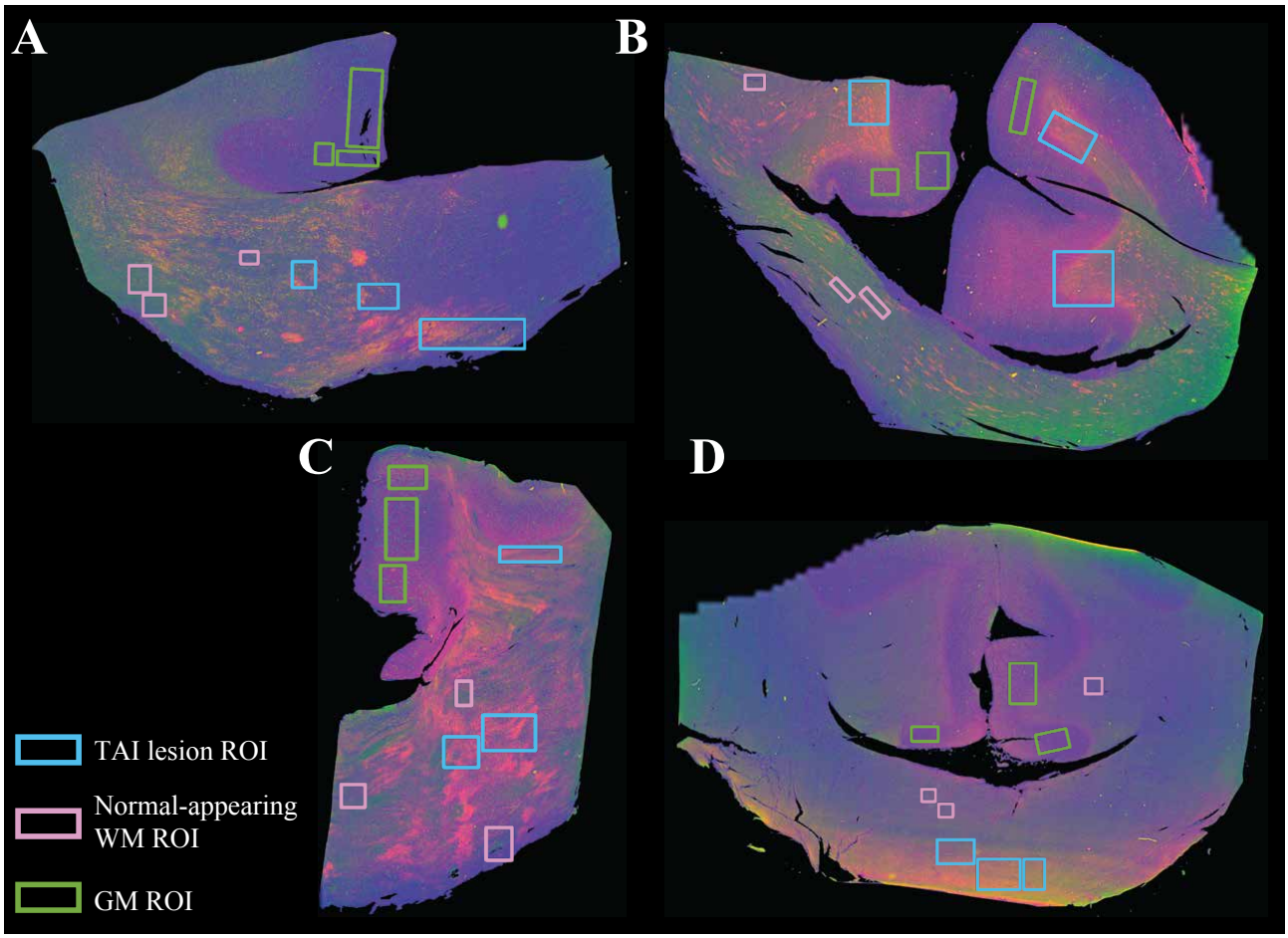

Figure S5: Deconvolved histological images of (A) Case 1, (B) Case 2, (C) Case 6, and (D) Case 4, with their defined regions of interest.

Supplementary Table 1: Main demographic and histopathological findings in TAI patients and controls

				Control vs. Nonfatal TBI	Control vs. Fatal TBI	Fatal TBI vs. Nonfatal TBI
Variable	Control, m=3	Nonfatal TBI, m=3	Fatal TBI, m=5	P	P	P
Median age, years (IQR)	52.0 (46.4, 53.6)	36.0 (32.5, 51.4)	49.0 (34.1, 59.9)	0.700	1.000	0.786[a]
Median brain weight, gr (IQR)	1294 (1268, 1623)	1469 (1361, 1572)	1540 (1512, 1642)	0.700	0.571	0.393[a]
Mean post-mortem interval, hours (SD)	23.4 (4.9)	12.0 (0.0)	15.3 (7.6)	0.057	0.121	0.386[b]
DAI grade, II	N/A	1 (33%)	3 (60%)	N/A	N/A	0.220[b]
APP-based TAI severity (in more severe side), +	N/A	2 (66%)	4 (80%)	N/A	N/A	0.588[b]
APP-based TAI extent, bilateral	N/A	0 (0%)	4 (80%)	N/A	N/A	0.1429[c]

[a]Mann-Whitney U-test; [b]unpaired two-tailed Student's t-test; [c]Fisher exact test

Supplementary Table 2: Comparisons of MRI parameters and pathological measures among control WM, mild TAI (mTAI), severe TAI (sTAI), normal-appearing WM in mTAI and sTAI tissue regions.

Variable	Control WM n=24	mTAI vs. Control WM		sTAI vs. Control WM		Normal-appearing WM in mTAI vs. Control WM		Normal-appearing WM in sTAI vs. Control WM	
	mean (SE)	Estimated mean difference (95% CI)	P P_{FDR}	Estimated mean difference (95% CI)	P P_{FDR}	Estimated mean difference (95% CI)	P P_{FDR}	Estimated mean difference (95% CI)	P P_{FDR}
T1-T2 SC, x100	0.78 (0.24)	3.31 (1.35, 5.27)	**0.001** **0.005**	3.92 (1.85, 5.99)	**<0.001** **<0.001**	0.31 (-0.59, 1.21)	0.502 1.000	-0.11 (-0.85, 0.63)	0.502 1.000
<D>-T1 SC, x100	0.52 (0.14)	-0.11 (-0.57, 0.32)	0.644 0.736	1.68 (0.40, 2.96)	**0.011** **0.023**	0.04 (-0.59, 0.67)	0.887 1.000	-0.06 (-0.52, 0.40)	0.887 1.000
<D>-T2 SC, x100	0.21 (0.17)	0.93 (0.35, 1.51)	**0.002** **0.005**	2.63 (1.31, 3.95)	**<0.001** **<0.001**	0.01 (-0.57, 0.59)	0.958 1.000	-0.02 (-0.52 0.48)	0.958 1.000
Adjusted FA	1.00 (0.05)	-0.06 (-0.53, 0.40)	0.790 0.790	-0.04 (-0.36, 0.27)	0.789 0.789	0.00 (-0.15, 0.15)	1.000 1.000	0.00 (-0.13, 0.13)	1.000 1.000
Adjusted MD	1.00 (0.05)	0.04 (-0.12, 0.20)	0.628 0.718	0.13 (-0.10, 0.36)	0.254 0.406	0.00 (-0.16, 0.16)	1.000 1.000	0.00 (-0.13, 0.13)	1.000 1.000
Adjusted T_1	1.00 (0.02)	-0.03 (-0.10, 0.04)	0.448 0.717	-0.04 (-0.17, 0.09)	0.519 0.593	0.00 (-0.07, 0.07)	1.000 1.000	0.00 (-0.06, 0.06)	1.000 1.000
Adjusted T_2	1.00 (0.03)	-0.09 (-0.19, 0.01)	0.077 0.155	-0.06 (-0.23, 0.11)	0.492 0.593	0.00 (-0.10, 0.10)	1.000 1.000	0.00 (-0.09, 0.09)	1.000 1.000
% area APP	0.18 (1.41)	20.49 (12.71, 28.27)	**<0.001** **<0.001**	26.46 (13.71, 39.22)	**<0.001** **<0.001**	0.22 (-4.56, 5.00)	0.929 1.000	0.79 (-3.30, 4.87)	0.929 1.000

Spectral component (SC); Fractional anisotropy (FA); mean diffusivity (MD)

References

Avram, A. V., Sarlls, J. E., Hutchinson, E., Basser, P. J., 2018. Efficient experimental designs for isotropic generalized diffusion tensor MRI (IGDTI). Magnetic Resonance in Medicine 79 (1), 180–194.

Benjamini, D., Basser, P., 2016. Use of marginal distributions constrained optimization (MADCO) for accelerated 2D MRI relaxometry and diffusometry. Journal of Magnetic Resonance 271, 40–45.

Benjamini, D., Basser, P. J., 2017. Magnetic resonance microdynamic imaging reveals distinct tissue microenvironments. NeuroImage 163, 183–196.

Benjamini, D., Basser, P. J., 2018. Towards clinically feasible relaxation-diffusion correlation MRI using MADCO. Microporous and Mesoporous Materials 269, 93–96.

Bland, M. J., Altman, D. G., 1986. Statistical methods for assessing agreement between two methods of clinical measurement. The Lancet 327 (8476), 307–310.

Pas, K., Komlosh, M. E., Perl, D. P., Basser, P. J., Benjamini, D., 2020. Retaining information from multidimensional correlation MRI using a spectral regions of interest generator. Scientific Reports 10 (1), 3246.